Lewis J. Gramer[1,2,*], Jun Zhang[1,2], Ghassan Alaka[2], Andrew Hazelton[1,2], Sundararaman Gopalakrishnan[2]

[1] - Cooperative Institute for Marine and Atmospheric Studies, Miami, FL 33149.

[2] - NOAA Atlantic Oceanographic and Meteorological Lab, Miami, FL 33149.

[*] - Corresponding author: Dr. Lew Gramer, 8930 Caribbean Blvd., Cutler Bay, FL 33157. Email: lew.gramer@noaa.gov. Telephone: +1-305-772-7933. ORCID: https://orcid.org/0000-0003-4772-1991

Key Points

1. Hurricanes approaching land tend to force downwelling over the ocean shelf;
2. Coastal downwelling sustains warmer sea-surface temperatures (SSTs) over the shelf;
3. Sustained SSTs and air-sea contrasts over the shelf increase enthalpy (heat and moisture) fluxes contributing directly to hurricane intensification near landfall, particularly for larger or slower-moving hurricanes.

Abstract

This study demonstrates a link between coastal downwelling and tropical cyclone (TC) intensification. We show coastal downwelling increases air-sea enthalpy (heat, moisture) fluxes ahead of TCs approaching land, creating conditions conducive to intensification even in the presence of typically inhibiting factors like strong vertical wind shear. The study uses a coupled TC model (HWRF-B) and buoy observations to demonstrate that coastal downwelling developed as three TCs in 2020 approached land. Results show that downwelling maintained warmer sea-surface temperatures over the ocean shelf, enhancing air-sea temperature/humidity contrasts. We found that in such cases the resulting air-sea enthalpy fluxes can replenish the boundary layer even when cool, dry air intrudes, as in sheared storms and storms approaching land. Warm, moist air advects into the inner core, enhancing convective development, thus providing energy for TC intensification. These results indicate coastal downwelling should be considered in forecasting TC intensity change before landfall.

Plain Language Summary

We examined forecasts for three hurricanes in 2020 that intensified near landfall. Using a coupled air-sea hurricane model, we found that tropical storm-force winds blowing parallel to the coast forced water near the ocean surface to move toward shore. Winds appear to often blow parallel to the coast when tropical

cyclones (hurricanes) are near land. The model showed that this onshore transport caused the water level to rise near the coastal boundary - a process called coastal Ekman convergence. This convergence forced water downward along the sloping seafloor and back away from shore, forming a circular exchange of water between the shelf and the open ocean; this exchange is called coastal downwelling. We demonstrate that incipient coastal downwelling brought warmer surface water over the shelf, heating and adding moisture to the air and thus providing more energy to these tropical cyclones. We further show that the additional energy provided by coastal downwelling can contribute to intensification of larger or slower-moving tropical cyclones before landfall. We suggest it is important to validate the modeling of coastal downwelling in future forecast models, in order to reliably forecast tropical cyclone intensity near landfall.

Index Terms: 3372, 4504, 4534, 4217, 4219

Keywords: landfalling hurricanes, coastal downwelling, shelf oceanography, rapid intensification, tropical cyclones, air-sea enthalpy flux

1. Introduction

In 2009 the National Oceanic and Atmospheric Administration (NOAA) established the 10-year Hurricane Forecast Improvement Program (HFIP; Gopalakrishnan et al. 2021) to improve the accuracy and reliability of hurricane forecasts and to extend forecast lengths (lead times) with increased certainty, especially before landfall. Predicting intensity changes in tropical cyclones (TCs), particularly rapid intensification (RI; Kaplan et al. 2015), is a complex, multiscale problem. This forecast guidance challenge assumes special significance when TCs intensify just before landfall. This paper introduces a previously unexplored mechanism by which some Atlantic TCs intensify prior to landfall, despite conditions generally deemed unfavorable for intensification.

Many studies have shown that high sea surface temperatures (SSTs) provide the necessary energy for TCs by increasing air-sea enthalpy (heat and moisture) fluxes, resulting in more sustained eyewall convection, a warmer core, a stronger pressure gradient between the center and the environment, and stronger winds in the eyewall region (Emanuel et al. 2004; Jaimes et al. 2015; Zhang et al. 2020a; Zhang et al. 2020b). Nevertheless, stronger near-surface winds can provide negative feedback on TC intensification in two ways, frictional dissipation, which is always present (Wang and Xu 2010; see Eq. S1) and SST cooling, which is dependent on air-sea interaction and ocean dynamics. SST cooling refers to the wake of cool surface water that TCs over the open ocean can create (e.g., Bender and Ginis 2000). Such wakes result from upwelling due to divergence of near-surface ocean currents and most importantly to rapid turbulent entrainment of cooler water into the oceanic mixed layer. The resultant SST cooling can significantly weaken TCs (Walker et al. 2014; Guo et al. 2020), particularly slower-moving (e.g., translation speed <2 m/s) and larger ones (radius of maximum winds ~50 km; Halliwell et al. 2015).

Environmental vertical wind shear (VWS) also weakens TCs through several processes (Wong and Chan 2004; Wang et al. 2015): vortex center misalignment (Kaplan et al. 2015), mid-tropospheric dry-air intrusion in the TC inner core (Bhalachandran et al. 2019; Tang and Emanuel 2010), upper-tropospheric divergent fluxes of entropy and potential energy (Riemer et al. 2010), and downdrafts carrying cool, dry air into the boundary layer (e.g., Bhalachandran et al., 2019; Riemer et al. 2010; Tang and Emanuel 2012). Forecasters typically expect TCs that are experiencing significant VWS to weaken, particularly TCs also impacted by ocean cooling.

When approaching landfall, however, TCs do sometimes intensify despite ocean mixing, the presence of VWS, and the negative effects of land interaction on the TC. In this study, we establish how three landfalling storms over the Caribbean Sea and the Gulf of Mexico intensified before landfall, and we specifically highlight the importance to that intensification of oceanographic processes over the coastal shelf. The three cases considered were landfalling TCs Sally, Hanna, and Eta from the 2020 season. The study used the ocean-coupled Basin-scale Hurricane Weather Research and Forecast (HWRF-B) system (Alaka et al. 2020) and observations collected from NOAA buoys to test three hypotheses:

1. TCs approaching land tend to force coastal downwelling over the ocean shelf.
2. Coastal downwelling sustains warmer SSTs over the shelf.
3. Sustained SSTs and resulting air-sea contrasts over the shelf enhance enthalpy fluxes that contribute directly to TC intensification near landfall, particularly for larger or slower-moving TCs.

2. Methods

The model in these case studies was the quasi-operational Basin-scale HWRF (HWRF-B; Zhang et al. 2016; Alaka et al. 2017, 2019, 2020) developed under HFIP. This model uses a fixed outer domain at 13.5 km horizontal resolution, with two TC-following nested domains at 4.5 and 1.5 km resolution, respectively. Up to five sets of nested domains can be deployed for a given initialization time to produce high-resolution forecasts for multiple TCs in the North Atlantic and eastern North Pacific. HWRF-B is coupled to MPIPOM-TC, an instance of the Princeton Ocean Model for TCs (Yablonsky et al. 2015) initialized with a two-day spinup from the Real-Time Ocean Forecasting System (RTOFS; Mehra and Rivin 2010).

Three TC case studies from the 2020 North Atlantic hurricane season were evaluated: Sally, Hanna, and Eta. Each TC experienced intensification while approaching land and interacted with the ocean shelf for a period of one day or more. To elucidate processes leading to intensification, model sea-surface fields were analyzed at forecast hours before and immediately after intensification. Supporting Information Table S1 details forecast initialization times for each

case and forecast hours chosen for detailed analysis: the forecast hour immediately following intensification and a forecast hour prior to intensification that was near the peak of both air-sea flux and storm kinetic energy (see below). We evaluated model currents and sea temperatures using quality-controlled buoy observations from the NOAA National Data Buoy Center (NDBC 2009; Winant et al. 1994).

We examined the relationship of air-sea fluxes to total storm kinetic energy and frictional dissipation using a model energy budget following Trenberth (1997) and Kato et al. (2016). See Supporting Information Equation S1 for details.

3. Results

Figure 1 shows the effect of downwelling-favorable winds over the shelf (i.e., TC surface winds >17.5 ms^{-1} blowing parallel to the coast with the coastline on their right) on near-surface ocean currents and sea-surface elevation. (We note that downwelling-favorable winds may be common when a TC is offshore of land.) These winds force surface Ekman transport toward the lateral boundary of the coast. This transport results in surface current convergence over time, causing a "bulge" in sea surface elevation over the shelf, in contrast with the sea-surface depression produced in the TC's wake. The bulge over the shelf is the precondition for coastal downwelling.

The right column of Figure 1 shows that after intensification, sea surface elevation for Sally (Fig. 1b) and Hanna (Fig. 1d) continued to increase dramatically. Approaching landfall, however, we note that storm surge also contributed to these elevation increases. For Eta, wind speed increase before landfall was small. However, surface Ekman convergence continued to increase through landfall (Fig. 1e,f), consistent with the other cases.

Figure 2 contrasts TC coastal downwelling effects on sea temperature and ocean currents with the effects of the TC wake in the open ocean: Coastal downwelling maintained warmer SSTs. In Sally (Fig. 2a), in particular, the shelf effect was apparent along the entire west Florida shelf following the storm's passage. In each storm's wake, by contrast, spatial variations in surface wind velocity within the storm caused Ekman divergence and upwelling while TC winds drove energetic mixed-layer deepening (see below), leading to SST cooling.

The middle column of Fig. 2 shows side views (vertical profiles) of coastal downwelling effects on temperature and ocean currents. Downwelling circulation advected warm water ashore and then downward, depressing ocean isotherms near the shelf. The black contour shows depression of the isotherm for 26 °C, a critical temperature threshold for TC intensification (Cione and Uhlhorn 2003; Cione 2015). Apparent in currents further from the shelf is an upward return flow, a characteristic of the cross-shelf circulation cell of coastal downwelling. For the two Gulf of Mexico storms (top and middle panels), the model shows low-salinity water derived from RTOFS initialization on the shelf (not shown). The resulting shelf stratification is consistent with intensified shoreward surface

transport and the quick development of the downwelling front (Csanady 2002; Austin and Lentz 2002).

The right column of Figure 2 shows profiles along a line from the inner core into each storm's wake. In contrast with the downwelling seen in the middle column, these profiles show the effects of upwelling and mixed-layer deepening, particularly on the 26 °C isotherm.

Figure S1 in the Supporting Information compares surface model temperatures with near-surface buoy observations from the Gulf of Mexico during Sally's passage. Sea temperatures from a deep-ocean buoy (Fig. S1b) showed a rapid decline of >1.5 °C d^{-1} during TC passage consistent with a developing cold wake, while multiple buoys on the shelf (Fig. S1c shows one example) recorded markedly slower declines of 0.2-0.4 °C d^{-1}, consistent with sustained SST from downwelling together with slower direct air-sea cooling.

Figure 3 shows all three storms had positive total (latent+sensible) air-sea enthalpy flux in the shelf region potentially aiding intensification despite moderate-to-strong deep-layer (i.e., 200-850 hPa) VWS and surface wind field asymmetries. The enthalpy fluxes prior to intensification (left panels) are more prominent over the shelf than the deeper ocean. Peak heat fluxes per grid-point for Sally, Hanna, and Eta were 1128, 1223, and 1570 Wm^{-2}, respectively, with all peaks occurring over the shelf. Enhanced fluxes over the shelf illustrate coastal downwelling's impact on air-sea temperature and humidity contrasts before intensification.

The asymmetries in these enhanced shelf fluxes led to initial asymmetries in surface winds. However, after intensification (right panels), these asymmetric fluxes counterintuitively led to a more symmetrized storm. While areas of substantial shelf enthalpy flux in all panels correspond with areas of large air-sea humidity and temperature contrast, they do not always correspond with areas of strongest winds (not shown). This supports the interpretation that shelf-based energy fluxes resulted from higher SSTs over the shelf rather than simple wind asymmetries.

Figure 4 shows that the boundary layer is replenished by the shelf air-sea enthalpy fluxes seen in Fig. 3, even when cool, dry air intrudes, as in strongly sheared storms like Sally and Eta. The figure shows cool, dry air with low equivalent potential temperature ($_e$) being carried by downdrafts into the boundary layer of each storm. Enthalpy fluxes in the boundary layer over the shelf replenish heat and moisture, increasing $_e$ between the left and right panels. During intensification, the higher- $_e$ air is transported along streamlines of surface air circulation toward the inner core of each storm. The transport of high-entropy air into the inner core enhances deep convection, resulting in symmetrization and intensification just before landfall.

Figures 3 and 4 show TC axisymmetrization and contraction, leading to intensification (Chen et al. 2018; Wadler et al. 2021). Fluxes from the shelf region together with boundary layer inflow enhance boundary layer entropy. When advected into the inner core, this leads to eyewall convection. This drives dia-

batic heating, which is favorable for symmetric intensification of the TC vortex (Chen et al. 2018), especially when it is located inside the radius of maximum winds (e.g. Vigh and Schubert 2009; Chen and Gopalakrishnan, 2015). All three storms were relatively slow-moving (Table S1), increasing the effect of the cold wake on fluxes over deeper water, while VWS enhanced the initial asymmetries; for both of these reasons, the subsequent intensification of each storm was remarkable.

In Figure 5, for each case we evaluate the simplified energy budget (Eq. S1). Change in the total kinetic energy and in maximum 10 m winds for all three storms is positively correlated with the difference between the total enthalpy fluxes and frictional dissipation. Note that enthalpy fluxes over the shelf region constituted an important fraction of the total flux (30-90%) leading up to and during intensification. The increase in kinetic energy lagged increases in surface flux by 6-12 h, supporting the argument that surface enthalpy fluxes are important for TC intensity change.

Significant increases in total enthalpy flux preceded intensification of 15 ms^{-1} in 36 h for Sally (Fig. 5a) and rapid intensification (Kaplan and DeMaria 2003) for Hanna (Fig. 5b), and the shelf effect contributed a majority of the total flux in both cases. Although Eta had intensified largely over the open ocean, it did encounter insular and continental shelf water starting in hour 72. And just before its first landfall during the time when it was approaching its maximum forecast intensity, 30-40% of its total enthalpy flux was derived from shelf waters (Fig. 5c). These shelf fluxes occurred in both the inner and outer core of Eta (see Fig. 3e). For all three cases, high enthalpy fluxes supported boundary-layer recovery of downdraft-induced low entropy air upshear before entering the updrafts in the downshear quadrant, countering the negative effect of ventilation on TC intensification.

4. Discussion and Conclusions

This paper investigated three hurricane case studies using the coupled HWRF-B / MPIPOM-TC modeling system. We found that these TCs forced coastal downwelling. Coastal downwelling develops when surface winds blow with the land to their right in the Northern Hemisphere (Sreenivas and Gnanaseelan 2014; Kuo et al. 2014; Shen et al. 2017; Zhang et al. 2019). We further found that coastal downwelling associated with each TC sustained SSTs over the shelf, consistent with other studies focused on non-TC conditions (e.g., Choboter et al. 2011). Shelf circulation during typhoons in the western north Pacific has also been observed to sustain SSTs (Kuo et al. 2014, Zhang et al. 2019, Zhang et al. 2021).

Here, however, we established a direct link between SST sustenance, enhanced enthalpy fluxes, and intensification for these three Atlantic TCs. Despite dry air intrusion due to persistent shear, enhanced air-sea enthalpy fluxes resulting from warmer SSTs over the shelf caused all three TCs to intensify before landfall.

Surface wind field forecasts and observations (not shown) indicated that warmer, moister air in the boundary layer was carried into each TC's inner core over a period of 6-12 h. In each of the three cases, an increase in total kinetic energy and intensification of surface winds both followed within another 6-12 h.

A simplified energy budget showed that a peak in residual of air-sea enthalpy flux minus frictional dissipation was correlated with a peak in TC intensity, similar to results for peak intensity found by Wang and Xu (2010). The lag of 12-18 h between peak air-sea enthalpy flux and peak TC intensity was consistent with idealized modeling studies (Halliwell et al. 2015). Our results support the conclusion that surface enthalpy fluxes are important for TC intensity change, constituting an energy source that is sufficient to compensate for the energy loss due to frictional dissipation (Emanuel 1986). Similarly, we find agreement with Zhang et al. (2017) that the importance of surface enthalpy fluxes for TC intensification hinges on the role they play in boundary-layer recovery. What is novel here is the importance of air-sea enthalpy fluxes due to TC-driven coastal downwelling in particular.

Future work will examine the relationship between shelf fluxes and storm structure (wind field sizes), as this may also constitute an important component of TC response to the shelf effect. Mechanisms for boundary-layer recovery within the TC core must also be explored in more detail in future, potentially using idealized studies. Finally, a recent study suggests that insolation differences related to cloud cover may be important for TC intensification near landfall (Lok et al. 2021): the energy budget discussed here will be extended to consider insolation as well as terms for potential and internal energy advection.

This study demonstrated that the coupled HWRF-B/MPIPOM-TC system appropriately modeled important coastal and shelf ocean dynamics related to TC intensification, namely the shelf effect due to coastal downwelling. We further showed that this oceanographic process can influence the boundary-layer recovery and atmospheric convection in intensifying TCs. These case studies represent three TCs from just one basin and hurricane season (2020 North Atlantic) that were impacted by coastal downwelling. Other cases from the 2017-2020 North Atlantic and eastern North Pacific hurricane seasons are being analyzed to confirm the relative prevalence of this shelf effect in causing landfalling TCs to intensify.

Future model-observational studies should analyze other oceanographic mechanisms that may contribute to the shelf effect as well, including coastal-trapped and continental shelf waves (Shen et al. 2021) and barrier-layer intensification (Balaguru et al. 2020, Rudzin et al. 2020). Implications of the shelf effect for TCs in a changing climate will also certainly bear further examination. Finally, future work must evaluate how the shelf effect can impact coastal communities and marine ecosystems, e.g., from enhanced bottom temperatures and cross-shore transport; such impacts may be significant (see, e.g., Dzwonkowski et al. 2020).

Above all, this study establishes the important role of coastal downwelling in increasing storm intensity before landfall. We recommend that modeling of the shelf effect be validated in future upgrades of operational coupled TC forecast models, such as those now under development by HFIP (Gall et al. 2013), in order to reliably forecast the intensity of landfalling TCs.

Acknowledgments

The authors wish to thank the Hurricane Forecast Improvement Program (HFIP) as well as funding from the Hurricane Supplemental (HSUP), NOAA Grant NA19OAR0220187. Internal review comments from F Marks, R Rogers, and R Lumpkin all improved the work. LJG is particularly thankful to lively recent discussions with HS Kim, and earlier discussions with SJ Monismith. Finally, suggestions from E Becker, L Albritton, K Nielsen, and N Deyo of the University of Miami all improved the clarity and concision of the manuscript.

Data

Graphical products associated with TC forecasts described in this text can be found online at:

https://storm.aoml.noaa.gov/

References

Alaka, G. J., D. Sheinin, B. Thomas, L. Gramer, Z. Zhang, B. Liu, H. S. Kim, and A. Mehra (2020), A hydrodynamical atmosphere/ocean coupled modeling system for multiple tropical cyclones, *Atmosphere*, *11*(8), 22.

Alaka, G. J., Jr., X. Zhang, S.G. Gopalakrishnan, S.B. Goldenberg, and F.D. Marks (2017). Performance of Basin-scale HWRF tropical cyclone track forecasts, *Weather and Forecasting*, *32*(3), 1253-1271, https://doi.org/10.1175/WAF-D-16-0150.1.

Alaka, G. J., Jr., X. Zhang, S.G. Gopalakrishnan, Z. Zhang, F.D. Marks, and R. Atlas (2019). Track uncertainty in high-resolution HWRF ensemble forecasts of Hurricane Joaquin, *Weather and Forecasting*, *34*(6), 1889-1908, https://doi.org/10.1175/WAF-D-19-0028.1.

Austin, J. A., and S. J. Lentz (2002), The inner shelf response to wind-driven upwelling and downwelling, *Journal of Physical Oceanography*, *32*(7), 2171-2193.

Balaguru, K., G. R. Foltz, L. R. Leung, J. Kaplan, W. W. Xu, N. Reul, and B. Chapron (2020), Pronounced Impact of Salinity on Rapidly Intensifying Tropical Cyclones, *Bulletin of the American Meteorological Society*, *101*(9), E1497-E1511.

Bender, M. A., and I. Ginis (2000), Real-case simulations of hurricane-ocean interaction using a high-resolution coupled model: Effects on hurricane intensity, *Monthly Weather Review*, *128*(4), 917-946.

Bhalachandran, S., Z. S. Haddad, S. M. Hristova-Veleva, and F. D. Marks (2019), The Relative Importance of Factors Influencing Tropical Cyclone Rapid Intensity Changes, *Geophysical Research Letters*, *46*(4), 2282-2292.

Chen, H., and S. G. Gopalakrishnan (2015), A study on the asymmetric rapid intensification of Hurricane Earl (2010) using the HWRF system, *Journal of the Atmospheric Sciences*, *72*(2), 531-550.

Chen, X. M., M. Xue, and J. Fang (2018), Rapid Intensification of Typhoon Mujigae (2015) under Different Sea Surface Temperatures: Structural Changes Leading to Rapid Intensification, *Journal of the Atmospheric Sciences*, *75*(12), 4313-4335.

Choboter, P. F., D. Duke, J. P. Horton, and P. Sinz (2011), Exact Solutions of Wind-Driven Coastal Upwelling and Downwelling over Sloping Topography, *Journal of Physical Oceanography*, *41*(7), 1277-1296.

Cione, J. J. (2015), The Relative Roles of the Ocean and Atmosphere as Revealed by Buoy Air-Sea Observations in Hurricanes, *Monthly Weather Review*, *143*(3), 904-913.

Cione, J. J., and E. W. Uhlhorn (2003), Sea surface temperature variability in hurricanes: Implications with respect to intensity change, *Monthly Weather Review*, *131*(8), 1783-1796.

Csanady, G. T. (1982), *Circulation in the coastal ocean*, 279 pp., D. Reidel Pub. Co.; Hingham, MA.

Dzwonkowski, B., J. Coogan, S. Fournier, G. Lockridge, K. Park, and T. Lee (2020), Compounding impact of severe weather events fuels marine heatwave in the coastal ocean, *Nature Communications*, *11*(1), 10.

Emanuel, K. A. (1986), An air sea interaction theory for tropical cyclones .1. Steady-state maintenance, *Journal of the Atmospheric Sciences*, *43*(6), 585-604.

Emanuel, K., C. DesAutels, C. Holloway, and R. Korty (2004), Environmental control of tropical cyclone intensity, *Journal of the Atmospheric Sciences*, *61*(7), 843-858.

Gall, R., J. Franklin, F. Marks, E. N. Rappaport, and F. Toepfer (2013), The Hurricane Forecast Improvement Project, *Bulletin of the American Meteorological Society*, *94*(3), 329-343.

Gopalakrishnan, S., et al. (2021), 2020 HFIP R&D Activities Summary: Recent Results and Operational Implementation, HFIP Technical Report: HFIP2021-1, https://hfip.org/sites/default/files/documents/hfip-annual-report-2020-final_0.pdf.

Halliwell, G. R., S. Gopalakrishnan, F. Marks, and D. Willey (2015), Idealized study of ocean impacts on tropical cyclone intensity forecasts, *Monthly Weather Review*, *143*(4), 1142-1165.

Jaimes, B., L. K. Shay, and E. W. Uhlhorn (2015), Enthalpy and Momentum Fluxes during Hurricane Earl Relative to Underlying Ocean Features, *Monthly Weather Review*, *143*(1), 111-131.

Kaplan, J., and M. DeMaria (2003), Large-scale characteristics of rapidly intensifying tropical cyclones in the North Atlantic basin, *Weather and Forecasting*, *18*(6), 1093-1108.

Kaplan, J., et al. (2015), Evaluating Environmental Impacts on Tropical Cyclone Rapid Intensification Predictability Utilizing Statistical Models, *Weather and Forecasting*, *30*(5), 1374-1396.

Kato, S., K. M. Xu, T. Wong, N. G. Loeb, F. G. Rose, K. E. Trenberth, and T. J. Thorsen (2016), Investigation of the Residual in Column-Integrated Atmospheric Energy Balance Using Cloud Objects, *Journal of Climate*, *29*(20), 7435-7452.

Kuo, Y. C., M. A. Lee, and C. S. Chern (2014), Typhoon-induced ocean responses off the southwest coast of Taiwan, *Ocean Dynamics*, *64*(11), 1569-1581.

Lok, C. C., J. C. Chan, and R. Toumi (2021), Tropical cyclones near landfall can induce their own intensification through feedbacks on radiative forcing, *Communications Earth & Environment*, *2*(1), 1-10.

Mehra, A., and I. Rivin (2010), A Real Time Ocean Forecast System for the North Atlantic Ocean, *Terrestrial Atmospheric and Oceanic Sciences*, *21*(1), 211-228.

NDBC (2009), Handbook of automated data quality control checks and procedures, https://www.ndbc.noaa.gov/qc.shtml *NOAA Rep.*, 78 pp.

Riemer, M., M. T. Montgomery, and M. E. Nicholls (2010), A new paradigm for intensity modification of tropical cyclones: thermodynamic impact of vertical wind shear on the inflow layer, *Atmospheric Chemistry and Physics*, *10*(7), 3163-3188.

Rudzin, J. E., S. Chen, E. R. Sanabia, and S. R. Jayne (2020), The Air-Sea Response During Hurricane Irma's (2017) Rapid Intensification Over the Amazon-Orinoco River Plume as Measured by Atmospheric and Oceanic Observations, *Journal of Geophysical Research-Atmospheres*, *125*(18), 21.

Shen, J. Q., Y. Qiu, S. W. Zhang, and F. F. Kuang (2017), Observation of Tropical Cyclone-Induced Shallow Water Currents in Taiwan Strait, *Journal of Geophysical Research-Oceans*, *122*(6), 5005-5021.

Shen, J. Q., S. W. Zhang, J. P. Zhang, M. Z. Zeng, and W. D. Fang (2021), Observation of continental shelf wave propagating along the eastern Taiwan Strait during Typhoon Meranti 2016, *Journal of Oceanology and Limnology*, *39*(1), 45-55.

Sreenivas, P., and C. Gnanaseelan (2014), Impact of Oceanic Processes on the Life Cycle of Severe Cyclonic Storm "Jal", *Ieee Geoscience and Remote Sensing Letters*, *11*(2), 519-523.

Tang, B., and K. Emanuel (2010), Midlevel ventilation's constraint on tropical cyclone intensity, *Journal of the Atmospheric Sciences*, *67*(6), 1817-1830.

Tang, B., and K. Emanuel (2012), Sensitivity of tropical cyclone intensity to ventilation in an axisymmetric model, *Journal of the Atmospheric Sciences*, *69*(8), 2394-2413.

Trenberth, K. E. (1997), Using atmospheric budgets as a constraint on surface fluxes, *Journal of Climate*, *10*(11), 2796-2809.

Vigh, J. L., and W. H. Schubert (2009). Rapid Development of the Tropical Cyclone Warm Core, *Journal of the Atmospheric Sciences*, *66*(11), 3335-3350.

Wadler, J. B., J. A. Zhang, R. F. Rogers, B. Jaimes, and L. K. Shay (2021), The Rapid Intensification of Hurricane Michael (2018): Storm Structure and the Relationship to Environmental and Air-Sea Interactions, *Monthly Weather Review*, *149*(1), 245-267.

Wang, Y. Q., and J. Xu (2010), Energy Production, Frictional Dissipation, and Maximum Intensity of a Numerically Simulated Tropical Cyclone, *Journal of the Atmospheric Sciences*, *67*(1), 97-116.

Wang, Y. Q., Y. J. Rao, Z. M. Tan, and D. Schonemann (2015), A Statistical Analysis of the Effects of Vertical Wind Shear on Tropical

Cyclone Intensity Change over the Western North Pacific, *Monthly Weather Review*, *143*(9), 3434-3453.

Winant, C., T. Mettlach, and S. Larson (1994), Comparison of buoy-mounted 75-kHz acoustic Doppler current profilers with vector-measuring current meters, *Journal of Atmospheric and Oceanic Technology*, *11*(5), 1317-1333.

Wong, M. L. M., and J. C. L. Chan (2004), Tropical cyclone intensity in vertical wind shear, *Journal of the Atmospheric Sciences*, *61*(15), 1859-1876.

Yablonsky, R. M., I. Ginis, B. Thomas, V. Tallapragada, D. Sheinin, and L. Bernardet (2015), Description and Analysis of the Ocean Component of NOAA's Operational Hurricane Weather Research and Forecasting Model (HWRF), *Journal of Atmospheric and Oceanic Technology*, *32*(1), 144-163.

Zhang, H., H. L. He, W. Z. Zhang, and D. Tian (2021), Upper ocean response to tropical cyclones: a review, *Geoscience Letters*, *8*(1), 12.

Zhang, J. A., J. J. Cione, E. A. Kalina, E. W. Uhlhorn, T. Hock, and J. A. Smith (2017), Observations of Infrared Sea Surface Temperature and Air-Sea Interaction in Hurricane Edouard (2014) Using GPS Dropsondes, *Journal of Atmospheric and Oceanic Technology*, *34*(6), 1333-1349.

Zhang, J. A., E. A. Kalina, M. K. Biswas, R. F. Rogers, P. Zhu, and F. D. Marks (2020a), A Review and Evaluation of Planetary Boundary Layer Parameterizations in Hurricane Weather Research and Forecasting Model Using Idealized Simulations and Observations, *Atmosphere*, *11*(10), 20.

Zhang, X., Gopalakrishnan, S. G., Trahan, S., Quirino, T. S., Liu, Q., Zhang, Z., Alaka, G., & Tallapragada, V. (2016). Representing Multiple Scales in the Hurricane Weather Research and Forecasting Modeling System: Design of Multiple Sets of Movable Multilevel Nesting and the Basin-Scale HWRF Forecast Application, *Weather and Forecasting*, *31*(6), 2019-2034, https://doi.org/10.1175/WAF-D-16-0087.1.

Zhang, Z., Y. Q. Wang, W. M. Zhang, & J. Xu (2019), Coastal Ocean Response and Its Feedback to Typhoon Hato (2017) Over the South China Sea: A Numerical Study, *Journal of Geophysical Research-Atmospheres*, *124*(24), 13731-13749.

Zhang, Z., W. M. Zhang, W. J. Zhao, and C. W. Zhao (2020b), Radial Distributions of Sea Surface Temperature and Their Impacts on the Rapid Intensification of Typhoon Hato (2017), *Atmosphere*, *11*(2), 24.

Figures

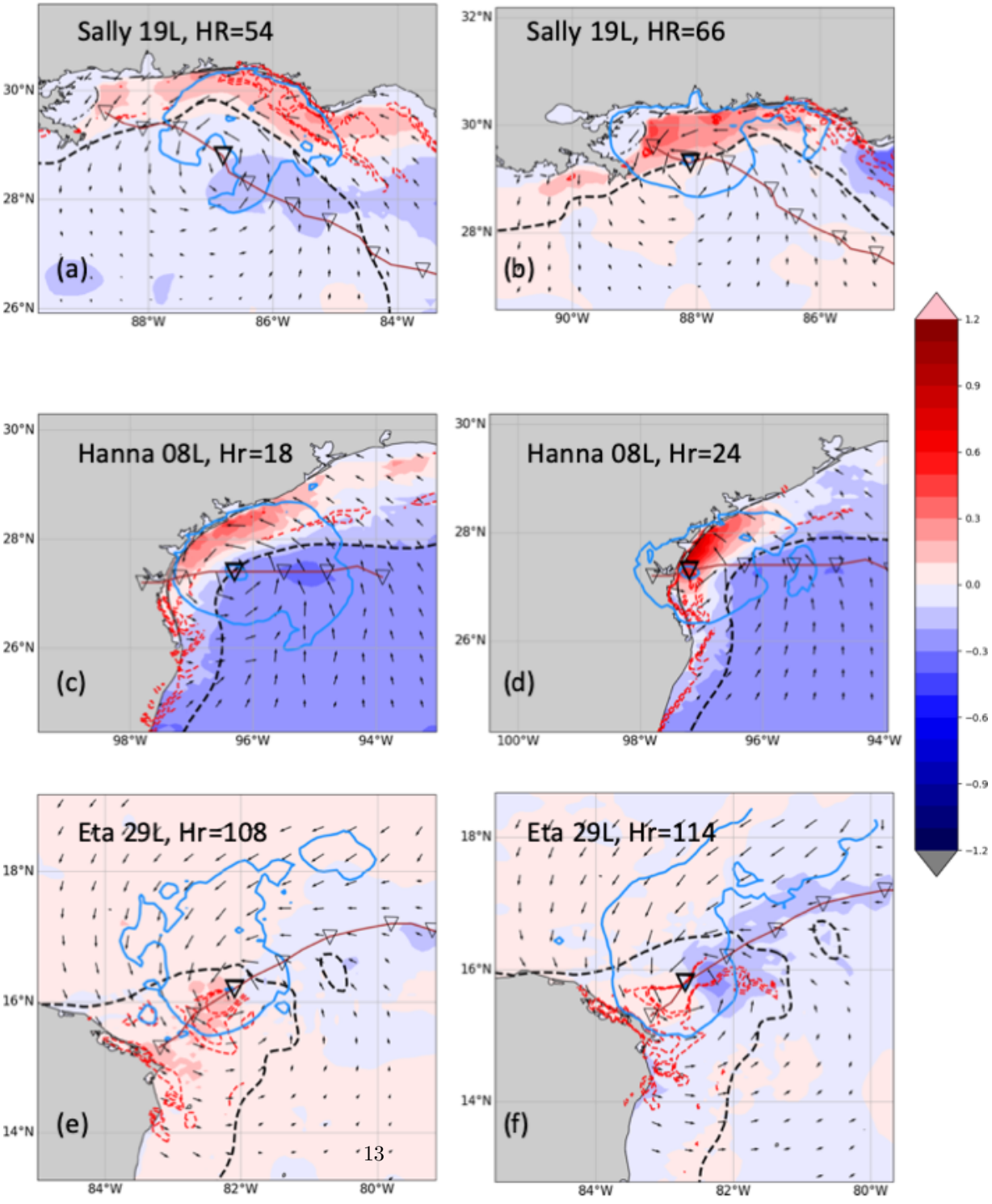
Sally 19L, HR=54
(a)
30°N
28°N
26°N
88°W
86°W
84°W
Sally 19L, HR=66
(b)
32°N
30°N
28°N
90°W
88°W
86°W
Hanna 08L, Hr=18
(c)
30°N
28°N
26°N
98°W
96°W
94°W
Hanna 08L, Hr=24
(d)
30°N
28°N
26°N
100°W
98°W
96°W
94°W
Eta 29L, Hr=108
(e)
18°N
16°N
14°N
84°W
82°W
80°W
Eta 29L, Hr=114
(f)
18°N
16°N
14°N
84°W
82°W
80°W
1.2
0.9
0.6
0.3
0.0
−0.3
−0.6
−0.9
−1.2

Figure 1: Ocean model fields for TCs (a,b) Sally, (c,d) Hanna, and (e,f) Eta, showing changes in sea surface elevation over time (m/day, shading), snapshots of instantaneous surface-current convergence (s^{-1}, dashed red contours), and 17.5 ms^{-1} (34 kt) surface wind fields (blue lines). Storm forecast tracks are in brown with triangle markers every 6 h. The left column shows a forecast hour prior to intensification: (a) hour 54, (c) hour 18, (e) hour 108. Right column shows the forecast hour immediately after intensification: (b) hour 66, (d) hour 24, (f) hour 114.

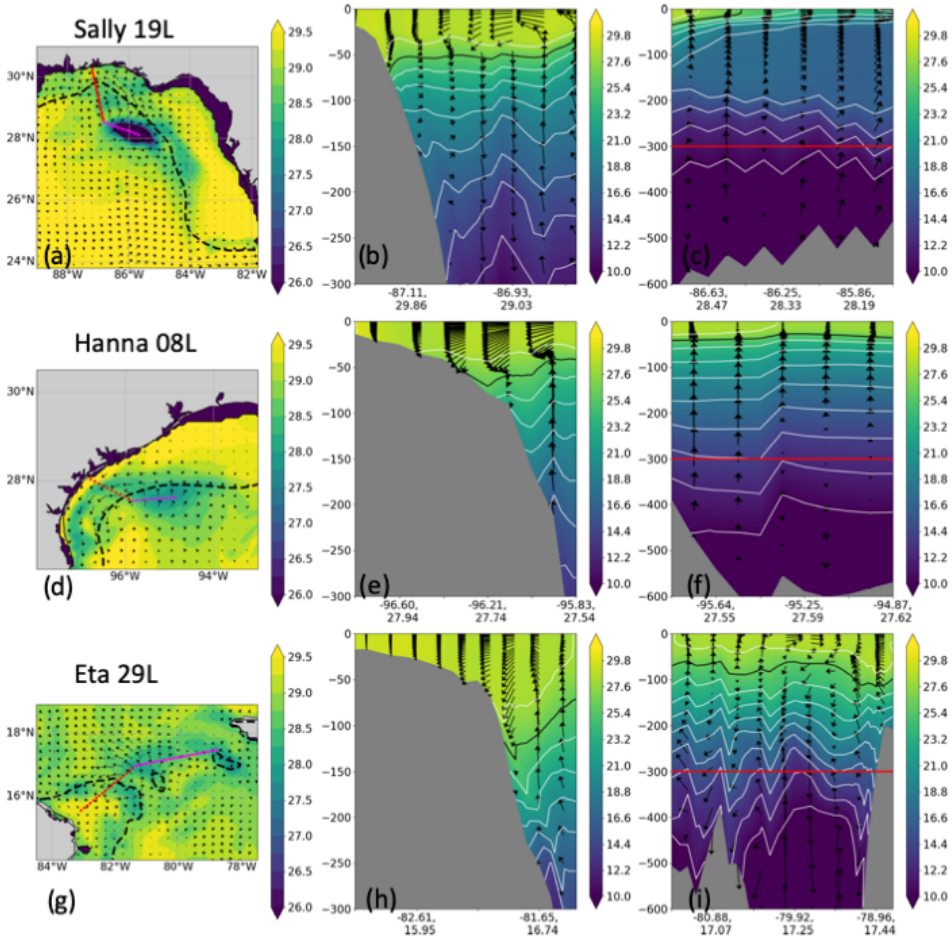

Figure 2: Ocean temperature and currents prior to intensification for: (a-c) Sally, (d-f) Hanna, and (g-i) Eta. Left panels (a,d,g) show sea surface temperature (SST, shading); black dashed contours show 150 m isobaths and black arrows show instantaneous ocean surface currents. Red lines show sections profiled in the middle column; magenta lines show sections profiled in the right

column. Middle panels (b,e,h) show cross-sections of sea temperature (shading) and along-track currents (black arrows) over coastal downwelling regions. Right panels (c,f,i) show cross-sections over the upwelling region in each storm's cold wake (red lines at 300 m highlight cutoff depth of panels in the middle column). White lines in the middle and right columns show sea temperature contours every 2 K; the contour of the 26 °C isobath is shown in black.

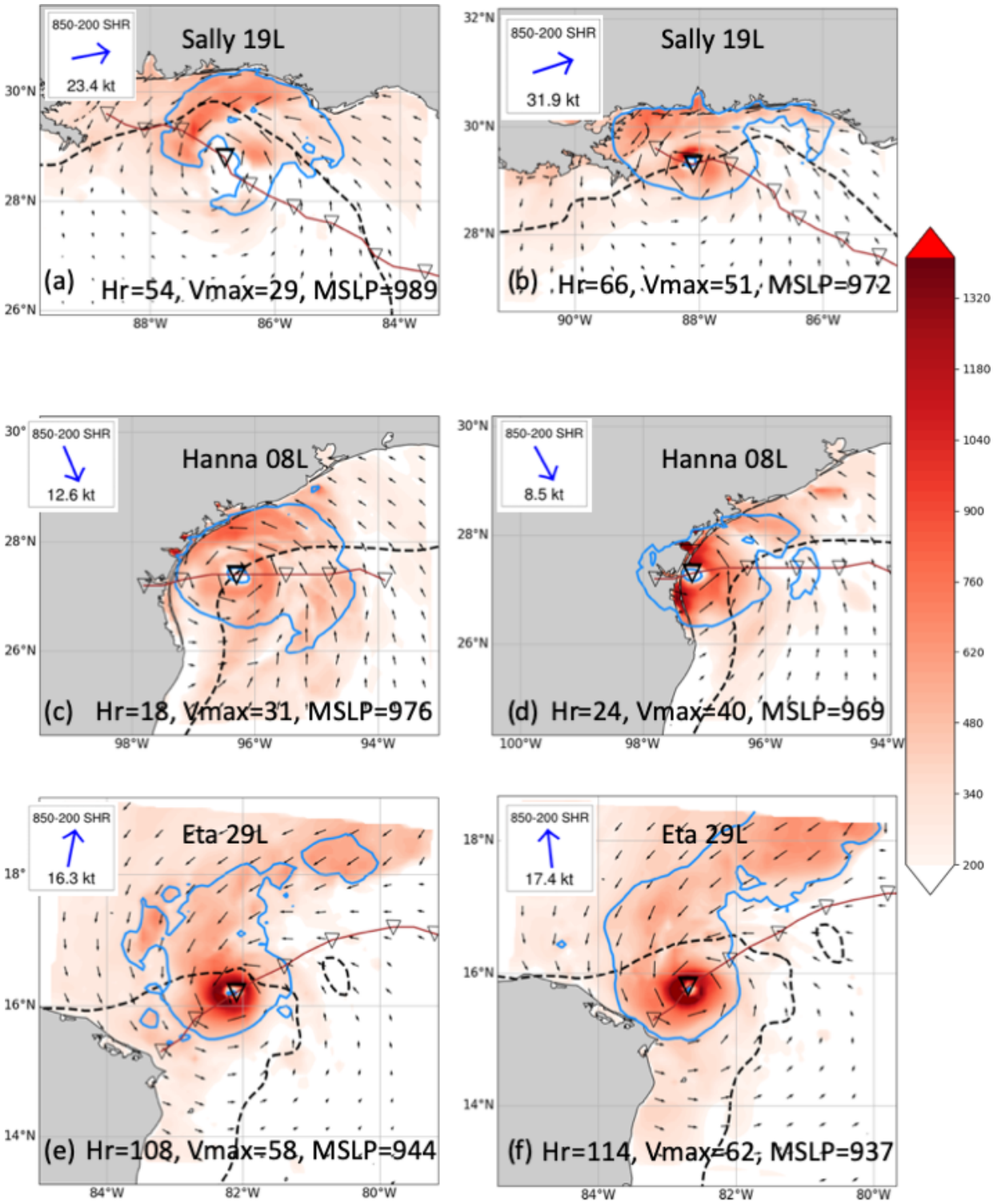
850-200 SHR
23.4 kt
Sally 19L
(a) Hr=54, Vmax=29, MSLP=989
850-200 SHR
31.9 kt
Sally 19L
(b) Hr=66, Vmax=51, MSLP=972
850-200 SHR
12.6 kt
Hanna 08L
(c) Hr=18, Vmax=31, MSLP=976
850-200 SHR
8.5 kt
Hanna 08L
(d) Hr=24, Vmax=40, MSLP=969
850-200 SHR
16.3 kt
Eta 29L
(e) Hr=108, Vmax=58, MSLP=944
850-200 SHR
17.4 kt
Eta 29L
(f) Hr=114, Vmax=62, MSLP=937
1320
1180
1040
900
760
620
480
340
200

Figure 3: Model forecast total air-sea enthalpy fluxes (W/m^2, shading), together with snapshots of instantaneous 17.5 ms^{-1} surface wind field (blue contours) and wind direction (black arrows), 150 m isobath (black dashed line), and forecast TC track (brown lines and triangles), for: (a) Sally, (b) Hanna, and (c) Eta. Insets show vertical wind shear between 850 and 200 mbar, maximum 10 m wind speed [ms^{-1}], and minimum sea-level pressure [hPa] at that forecast hour.

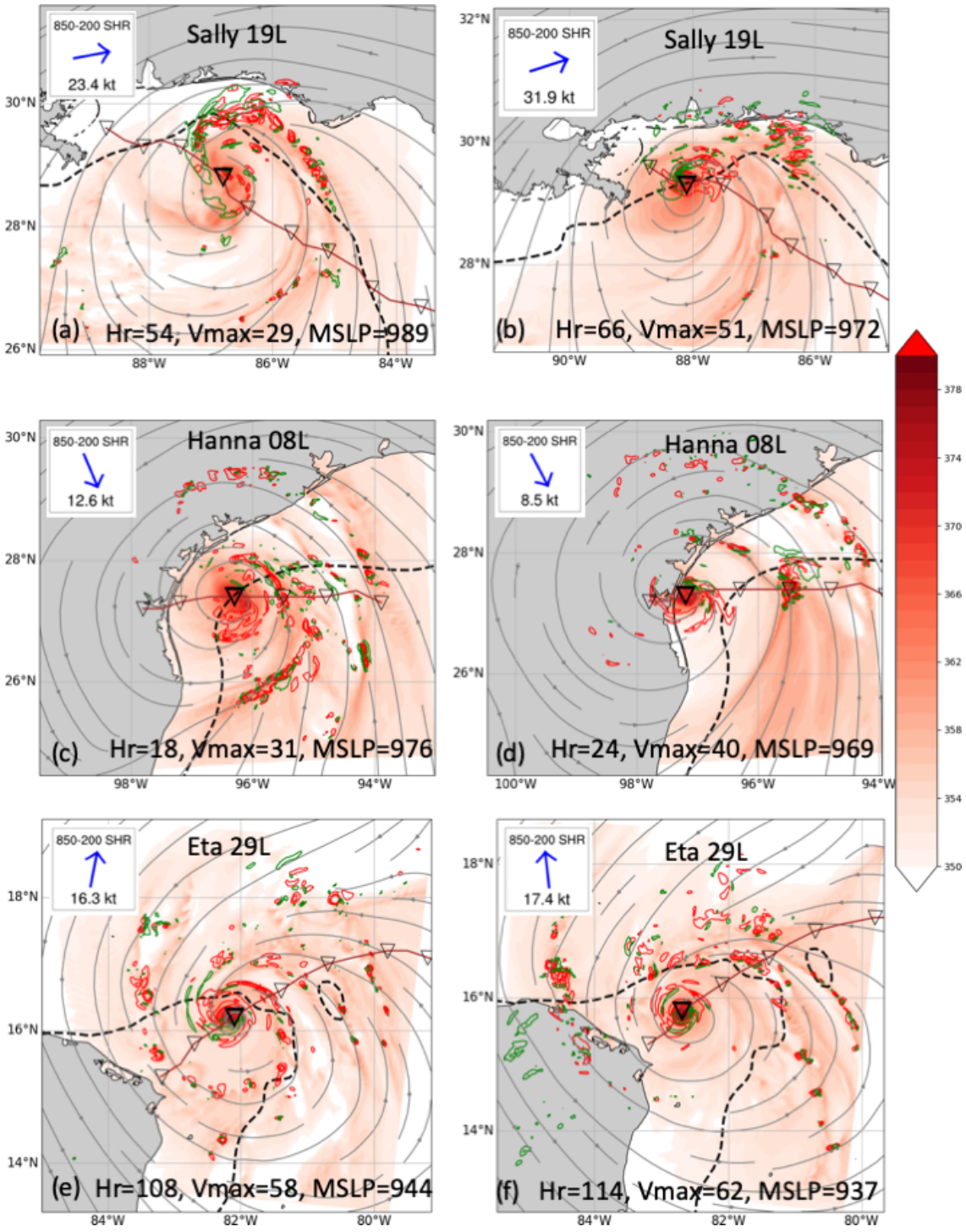
850-200 SHR
23.4 kt
Sally 19L
(a) Hr=54, Vmax=29, MSLP=989
850-200 SHR
31.9 kt
Sally 19L
(b) Hr=66, Vmax=51, MSLP=972
850-200 SHR
12.6 kt
Hanna 08L
(c) Hr=18, Vmax=31, MSLP=976
850-200 SHR
8.5 kt
Hanna 08L
(d) Hr=24, Vmax=40, MSLP=969
850-200 SHR
16.3 kt
Eta 29L
(e) Hr=108, Vmax=58, MSLP=944
850-200 SHR
17.4 kt
Eta 29L
(f) Hr=114, Vmax=62, MSLP=937
378
374
370
366
362
358
354
350

Figure 4: Mean equivalent potential temperature ($_e$,shading), vertical velocity (contours) and mean wind streamlines below 850 mb. Green contours denote downdrafts (below 600 mb) while red contours denote updrafts (above 600 mb). Left and right columns show periods before and after intensification, respectively. Insets show vertical wind shear between 850 and 200 mbar, maximum 10 m wind speed [ms^{-1}], and minimum sea-level pressure [hPa].

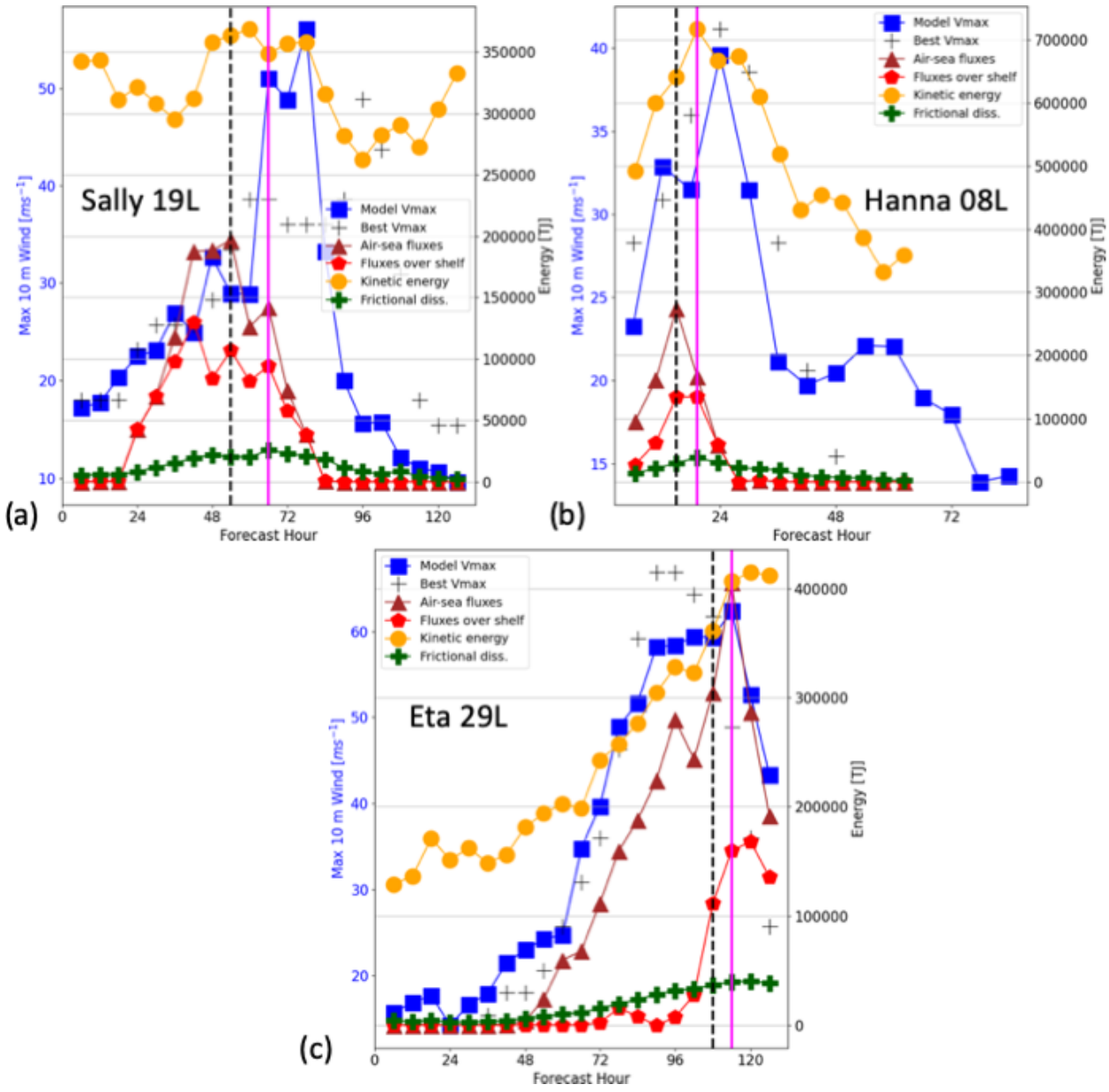

Figure 5: Components of the simplified energy budget (Eq. S1) in TJ (scale shown in the black axis at right of each panel) including terms for total air-sea enthalpy flux (THF_d+THF_s, brown lines, triangles), enthalpy flux over the shelf only (THF_s, red line, pentagons), frictional dissipation (FD, green lines and "+"), and total kinetic energy (KE, orange lines, circles). Maximum 10 m wind speed in ms^{-1} is shown in the blue axis at left (blue line, square markers), along with best-track maximum speed (black "+"). Panels show: (a) Sally, (b) Hanna, and (c) Eta. Note the differing vertical scales between panels.